UNIGRAZ-UTP 15-04-96

WU B 96-13

Exclusive Photoproduction of Large Momentum-Transfer K and K* Mesons

P. Kroll* and M. Schürmann**

Fachbereich Physik, Universität Wuppertal, D-42097 Wuppertal, Germany

K. Passek+

Rudjer Bošković Institute, P.O. Box 1016, HR-10000 Zagreb, Croatia

W. Schweiger++

Institut für Theoretische Physik, Universität Graz, A-8010 Graz, Austria

(April 15, 1996)

Abstract

The reactions $\gamma p \longrightarrow K^+\Lambda$ and $\gamma p \longrightarrow K^{*+}\Lambda$ are analyzed within perturbative QCD, allowing for diquarks as quasi-elementary constituents of baryons. The diquark-model parameters and the quark-diquark distribution amplitudes of proton and Lambda are taken from previous investigations of electromagnetic baryon form factors and Compton-scattering off protons. Unpolarized differential cross sections and polarization observables are computed for different choices of the K and K* distribution amplitudes. The asymptotic form of the K distribution amplitude ($\propto x_1 x_2$) is found to provide a satisfactory description of the K photoproduction data.

13.60.Le, 12.38.Bx

I. INTRODUCTION

The reactions γp $\rightarrow KY$ (Y=Λ,Σ) belong to the most elementary processes which allow to study strangeness production. Stimulated by the advent of a new generation of intermediate energy electron facilities, like ELSA or CEBAF, they recently received renewed interest. Traditional hadronic models applied to the analysis of K photoproduction mostly make use of Feynman-diagram techniques [1–3]. The corresponding reaction mechanism is based on the exchange of p, Λ, Σ, K, and K*, along with a varying number of N* and Y* resonances. Apart from some problems with SU(3) bounds on the hadronic coupling constants $g_{\rm KYN}$ [4], such models seem to work properly for photon energies up to $p^{\gamma}_{\rm lab}\lesssim 1.4-2.2$ GeV. New data of higher precision and completeness (which include also spin observables) [5,6] are expected to restrict still persisting uncertainties in the meson-baryon couplings and the resonance parameters.

A more fundamental treatment of photoproduction should, of course, rely on QCD, the dynamics of interacting quarks and gluons. A step in this direction are effective, "QCD-inspired" models which include already one or the other feature of QCD. A particular example is the chiral quark model which has been applied to K photoproduction very recently [7]. Its elementary degrees of freedom are constituent quarks and the members of the (lowest lying) pseudoscalar meson octet (K, η, and π). The latter are considered as Goldstone bosons associated with the spontaneous breaking of chiral symmetry. The Goldstone bosons couple directly to the (confined) quarks . With less parameters than hadronic approaches this model also provides reasonable results for $p^{\gamma}_{\rm lab}\lesssim 2$ GeV. Its restricted range of validity is caused by the use of non-relativistic transition operators and baryon wave functions.

Direct application of QCD is (till now) restricted to kinematical situations in which the scattering of the hadronic constituents and their hadronization takes place on rather different scales. In general this means large energies and momentum transfers ($p_\perp$). Well beyond the resonance region ($p^{\gamma}_{\rm lab} \gg 1$ GeV) exclusive photoproduction cross sections exhibit a characteristic angular dependence. At forward (small t) and backward (small u) angles the

strong variation of the differential cross section is adequately reproduced by the exchange of meson and baryon Regge trajectories, respectively [8]. Around $\theta_{\rm cm} = 90^\circ$ (large t and u) the cross section flattens and shows (for fixed angles) an energy dependence typical for a hard interaction between the photon and the constituents inside the proton. A constituent scattering model for high-energy, large-$p_\perp$ elastic and quasielastic reactions has been proposed in Ref. [9]. The interaction mechanism of this model, namely quark interchange, may be also thought of as one of the simplest ways to describe photoproduction of open strangeness. The resulting interchange amplitude is just a convolution over light-cone wave functions of the interacting quarks, which have to be parameterized in an appropriate way.

A more subtle picture, often called the "hard-scattering approach ", emerges if one tries to figure out the leading twist contributions to hard exclusive processes within perturbative QCD [10]. The outcome of such an analysis is a factorization formula which is also expressed as a convolution integral. This integral now consists of distribution amplitudes (DAs) and a hard scattering amplitude. The process dependent hard scattering amplitude is perturbatively calculable and represents the scattering of the hadronic constituents in collinear approximation. The process independent DAs contain the non-perturbative bound-state dynamics of the hadronic constituents. DAs are, roughly speaking, valence Fock-state wave functions integrated over the transverse momentum. At present, the knowledge on hadron DAs is still rather limited. The main information is provided by QCD sum-rule techniques which give estimates of the lowest moments of various meson and baryon DAs [11–13]. The few lowest moments impose some restrictions on the shape of the DAs but do not determine them uniquely. A thorough discussion on how to construct model DAs reproducing a certain number of moments can be found in Ref. [14]. One should also note that the DAs constrained by QCD sum rules are subject to severe criticism [15–18]. Thus one is forced, at present, to supplement the lack of theoretical knowledge on DAs by some input coming from experiment. Photoproduction reactions are, in this respect, certainly very interesting. They exhibit a rich flavour structure and are still simple enough to allow for the computation of all the Feynman diagrams which enter the hard scattering amplitude. Perturbative QCD

predictions for various photoproduction channels have been published in Ref. [19]. This paper discusses also the sensitivity of the results on the choice of the hadron DAs. Apart from the fact that there are objections to the numerics of this work (cf. Sect. IV) and it still needs confirmation, the predictions for the K-Λ channel occur to be in considerable disagreement with experiment.

The present work concentrates on photoproduction of the K-Λ and K*-Λ final states. We consider these reactions within a particular version of the hard-scattering approach in which baryons are treated as quark-diquark systems. The same approach has already been applied successfully to other photon-induced hadronic reactions like magnetic and electric baryon form factors in the space- [20] and time-like region [21], real and virtual Compton scattering [22], and two-photon annihilation into proton-antiproton [21]. Further applications of the diquark model include the charmonium decay $\eta_c \to p\bar{p}$ [21] and the calculation of Landshoff contributions in elastic proton-proton scattering [23]. The introduction of diquarks does not only simplify computations, but is rather motivated by the requirement to extend the hard-scattering approach from large down to intermediate momentum transfers ($p_\perp^2 \gtrsim 4$ GeV^2). This is the momentum-transfer region where experimental data are still available, but where still persisting non-perturbative effects prevent the pure quark hard-scattering approach to become fully operational. Diquarks may be considered as an effective way to cope with such non-perturbative effects. It is an assumption that, on an intermediate momentum-transfer scale, two of the three valence quarks in a baryon make up a diquark cluster. However, from many experimental and theoretical approaches there have been indications suggesting the presence of diquarks. For instance, they were introduced in baryon spectroscopy, in nuclear physics, in jet fragmentation and in weak interactions to explain the famous $\Delta I = 1/2$ rule. Diquarks also provide a natural explanation of the equal slopes of meson and baryon Regge trajectories. For more details and for references, see [24]. It is important to note that QCD provides some attraction between two quarks in a colour $\{\bar{3}\}$ state at short distances as is to be seen from the static reduction of the one-gluon exchange term. Also the instanton force seem to lead to diquark formation [25]. Even more important for our aim, diquarks

have also been found to play a role in inclusive hard-scattering reactions. The most obvious place to signal their presence is deep inelastic lepton-nucleon scattering. Indeed the higher twist terms, convincingly observed [26], can be modeled as lepton-diquark elastic scattering. Baryon production in inclusive p-p collisions also clearly reveals the need for diquarks scattered elastically in the hard elementary reactions [27]. For instance, kinematical dependencies or the excess of the proton yield over the antiproton yield find simple explanations in the diquark model. No other explanation of these phenomena is known as yet.

The main ingredients of the diquark model are baryon DAs in terms of quarks and diquarks, the coupling of gluons and photons to diquarks, and, in order to account for the composite nature of diquarks, phenomenological diquark form factors. The proper choice of the diquark form factors guarantees the compatibility of the diquark model with the pure quark hard-scattering approach in the limit $p_\perp \to \infty$. In so far the pure quark picture of Brodsky-Lepage and the diquark model do not oppose each other, they are not alternatives but rather complements. The model parameters have been determined in Ref. [20] by means of elastic electron-nucleon scattering data. The full model incorporates scalar (S) and vector diquarks. Vector diquarks are important for the description of spin observables which violate hadronic helicity conservation, i.e. quantities not explicable within the pure quark hard-scattering approach. The nice and simplifying feature of the two photoproduction reactions we are interested in is that they are not influenced by vector diquarks since only the $S_{[u,d]}$ diquark is common to proton and Λ.

The following section starts with an outline of the hard-scattering approach with (scalar) diquarks. It contains also a description of the Kaon, proton, and Λ DAs to be used in the sequel. Section III deals with the constituent kinematics, photoproduction observables, and the general structure of photoproduction helicity amplitudes within the diquark model. Predictions for photoproduction observables with a discussion of their dependence on the choice of the Kaon DA can be found in Sec. IV. Conclusions and prospects are given in Sec. V. Analytical expressions for the helicity amplitudes are tabulated in Appendix A. Our numerical method for treating propagator singularities is sketched in Appendix B.

II. HARD SCATTERING WITH DIQUARKS

Within the hard-scattering approach a helicity amplitude $M_{\{\lambda\}}$ for the reaction $\gamma \mathrm{p} \longrightarrow \mathrm{K}^{(*)+}\Lambda$ is (to leading order in $1/p_\perp$) given by the the convolution integral [10]

$$M_{\{\lambda\}}(\hat{s},\hat{t}) = \int_0^1 dx_1 dy_1 dz_1 \phi^{\mathrm{K}^{(*)}\,\dagger}(z_1,\tilde{Q}) \phi^{\Lambda\,\dagger}(y_1,\tilde{Q}) \widehat{T}_{\{\lambda\}}(x_1,y_1,z_1;\hat{s},\hat{t}) \phi^{\mathrm{p}}(x_1,\tilde{Q})\,. \qquad (2.1)$$

The distribution amplitudes ϕ^{H} are probability amplitudes for finding the valence Fock state in the hadron H with the constituents carrying certain fractions of the momentum of their parent hadron and being collinear up to a factorization scale $\tilde{Q}$. In our model the valence Fock state of an ordinary baryon is assumed to consist of a quark and a diquark (D). We fix our notation in such a way that the momentum fraction appearing in the argument of ϕ_{H} is carried by the quark – with the momentum fraction of the other constituent (either diquark or antiquark) it sums up to 1 (cf. Fig. 1). In what follows we will neglect the (logarithmic) $\tilde{Q}$ dependence of the DAs since it is of minor importance in the restricted energy range we will be interested in. The hard scattering amplitude $\widehat{T}_{\{\lambda\}}$ is calculated perturbatively in collinear approximation and consists in our particular case of all possible tree diagrams contributing to the elementary scattering process $\gamma \mathrm{uS} \longrightarrow \mathrm{u\bar{s}sD}$. A few examples of such diagrams are depicted in Fig. 2. The subscript $\{\lambda\}$ represents the set of possible photon, proton and Λ helicities. We have written the Mandelstam variables s and t with a hat to indicate that masses are neglected during the calculation of the hard scattering amplitude. They are only taken into account in flux and phase-space factors.

If one assumes zero relative orbital angular momentum between quark and diquark and takes advantage of the collinear approximation ($p_{\mathrm{q}} = x_1 p_{\mathrm{B}}$ and $p_{\mathrm{D}} = x_2 p_{\mathrm{B}} = (1-x_1) p_{\mathrm{B}}$) the valence Fock-state wave function of a baryon B belonging to the energetically lowest lying octet may be written as

$$\Psi^{\mathrm{B}}(p_{\mathrm{B}};\lambda) = f_{\mathrm{S}}^{\mathrm{B}} \phi_{\mathrm{S}}^{\mathrm{B}}(x_1)\, \chi_{\mathrm{S}}^{\mathrm{B}}\, u(p_{\mathrm{B}},\lambda) + f_{\mathrm{V}}^{\mathrm{B}}\, \phi_{\mathrm{V}}^{\mathrm{B}}(x_1)\, \chi_{\mathrm{V}}^{\mathrm{B}}\, \frac{1}{\sqrt{3}} \left(\gamma^\alpha + \frac{p_{\mathrm{B}}^\alpha}{m_{\mathrm{B}}}\right) \gamma_5 u(p_{\mathrm{B}},\lambda)\,. \qquad (2.2)$$

The two terms in Eq. (2.2) represent configurations consisting of a quark and either a scalar or vector diquark. The pleasant feature of the covariant wave-function representation

Eq.(2.2) is that it contains, besides x_1 and α (the Lorentz index of the vector-diquark polarization vector), only baryonic quantities (momentum $p_{\rm B}$, helicity λ, baryon mass $m_{\rm B}$).

For an SU(6)-like spin-flavour dependence the flavour functions χ for proton and Λ take on the form (the notation should be obvious)

$$\chi_{\rm S}^{\rm p} = {\rm uS}_{\rm [u,d]}\,, \quad \chi_{\rm V}^{\rm p} = \quad [{\rm uV}_{\rm \{u,d\}} - \sqrt{2}{\rm dV}_{\rm \{u,u\}}]/\sqrt{3}\,, \tag{2.3}$$

$$\chi_{\rm S}^{\Lambda} = [{\rm uS}_{\rm [d,s]} - {\rm dS}_{\rm [u,s]} - 2{\rm sS}_{\rm [u,d]}]/\sqrt{6}\,, \quad \chi_{\rm V}^{\Lambda} = [{\rm uV}_{\rm \{d,s\}} - {\rm dV}_{\rm \{u,s\}}]/\sqrt{2}\,. \tag{2.4}$$

Similarly, also the q-$\bar{\rm q}$ wave functions of pseudoscalar (PM) and vector (VM) mesons may be represented in a covariant way

$$\Psi^{\rm PM}(p_{\rm PM}) = f^{\rm PM}\,\phi^{\rm PM}(x_1)\,\chi^{\rm PM}\,\frac{1}{\sqrt{2}}(\not{p}_{\rm PM} + m_{\rm PM})\gamma_5\,, \tag{2.5}$$

$$\Psi^{\rm VM}(p_{\rm VM};\lambda) = -f^{\rm VM}\,\phi^{\rm VM}(x_1,\lambda)\,\chi^{\rm VM}\,\frac{1}{\sqrt{2}}(\not{p}_{\rm VM} + m_{\rm VM})\;\not{\epsilon}(\lambda)\,, \tag{2.6}$$

with the flavour function of the $\rm K^{(*)+}$ meson given by

$$\chi^{\rm K^{(*)+}} = {\rm u}\bar{\rm s}\,. \tag{2.7}$$

At this point we are already in the position to recognize a considerable simplification in the treatment of the reaction $\gamma{\rm p} \longrightarrow {\rm K^{(*)+}}\Lambda$ as compared to arbitrary photoproduction processes. Photoproduction of the $\rm K^{(*)+}$-Λ final state can solely proceed via the $\rm S_{[u,d]}$ diquark. This is the only kind of diquark occurring in both, the proton and the Λ wave function (cf. Eqs. (2.3) and (2.4)). The opposite situation, namely that only the $\rm V_{\{u,d\}}$ diquark becomes involved, holds for $\gamma{\rm p} \longrightarrow {\rm K^{(*)+}}\Sigma^0$. The fact that scalar diquarks as well as (massless) quarks do not change their helicity when interacting with a gluon imposes already strong restrictions on spin observables of the $\rm K^+$-Λ and $\rm K^{*+}$- Λ channels. Helicity amplitudes which require the flip of the baryonic helicity are predicted to vanish, e.g., for the $\gamma{\rm p} \longrightarrow {\rm K^+}\Lambda$ process. On the other hand, helicity flips may take place in the $\gamma{\rm p} \longrightarrow {\rm K^+}\Sigma^0$ reaction by means of the vector diquark. In order to work out the different features of scalar

and vector diquarks a comparison of the Λ and Σ^0 photoproduction channels would certainly be of great benefit.

The complicated, non-perturbative bound-state dynamics is contained in the DAs $\phi^{\rm H}$. These are light-cone wave functions integrated over transverse momentum (up to $\tilde{Q}$). The $r = 0$ values of the corresponding configuration space wave functions are related to the constants $f^{\rm H}$. We will check the sensitivity of our photoproduction calculation on the shape of the K (K*) DA by choosing two qualitatively rather different forms: the one is the asymptotic DA

$$\phi_{\rm asy}(x) = 6x(1-x) \; , \tag{2.8}$$

which solves the $\tilde{Q}$ evolution equation for $\phi(x,\tilde{Q})$ in the limit $\tilde{Q} \to \infty$ (see, e.g., Ref. [10]); the other one is a two-humped DA, namely

$$\phi^{\rm K}_{\rm CZ}(x) = N^{\rm K}\phi_{\rm asy}(x)[0.08 + 0.6(1-2x)^2 + 0.25(1-2x)^3] \; , \tag{2.9}$$

for the K,

$$\phi^{\rm K^*}_{\rm L}(x) = N^{\rm K^*}_{\rm L}\phi_{\rm asy}(x)[0.18 + 0.1(1-2x)^2 + 0.41(1-2x)^3] \; , \tag{2.10}$$

for the longitudinally polarized K*, and

$$\phi^{\rm K^*}_{\rm T}(x) = N^{\rm K^*}_{\rm T}\phi_{\rm asy}(x)[0.284 + 0.07(1-2x) - 0.534(1-2x)^2 + 0.21(1-2x)^3 + 0.267(1-2x)^4] \; , \tag{2.11}$$

for the transversially polarized K*. The DAs, Eqs. (2.9)-(2.11), have been proposed in Refs. [11] and [29]. They reproduce the corresponding QCD sum-rule moments at $\tilde{Q}^2 = 0.25$ GeV^2. It has been demonstrated quite recently that the linear x-dependence of pseudoscalar meson DAs at the end points $x \to 0, 1$ can be considered as a direct consequence of QCD [30].

The usual normalization condition, $\int_0^1 dx \phi^{\rm H}(x) = 1$, fixes the constants N in Eqs. (2.9)-(2.11). The quantities $f^{\rm PM}$ and $f^{\rm VM}$ showing up in Eqs. (2.5) and (2.6) are related to

experimentally determinable decay constants of the corresponding mesons. From the $K^+ \to \mu^+\nu_\mu$ decay one infers in particular that $f^{K^+} = f^{K^+}_{\rm decay}/2\sqrt{6} = 32.6$ MeV. The value of f^{K^*} is only known indirectly via the QCD-sum-rule result $f^{K^*} = 1.05 f^\rho$ (cf. Ref. [11]). The experimental value of $f^\rho = f^\rho_{\rm decay}/2\sqrt{6} = 40.8$ MeV obtained from the $\rho^0 \to e^+e^-$ decay implies $f^{K^*} = 42.9$ MeV.

In previous applications of the diquark model [20–22] a DA of the form

$$\phi^{\rm B}_{\rm S}(x) = N_{\rm S} x(1-x)^3 \exp\left[-b^2\left(\frac{m_{\rm q}^2}{x} + \frac{m_{\rm S}^2}{(1-x)}\right)\right] , \tag{2.12}$$

proved to be quite appropriate for the quark-scalar diquark Fock state of octet baryons B. The origin of the DA, Eq. (2.12), is a nonrelativistic harmonic-oscillator wave function [31]. Therefore the masses appearing in the exponentials have to be considered as constituent masses (330 MeV for light quarks, 580 MeV for light diquarks, strange quarks are 150 MeV heavier than light quarks). The oscillator parameter $b^2 = 0.248$ GeV^{-2} is chosen in such a way that the full wave function gives rise to a value of 600 MeV for the mean intrinsic transverse momentum of quarks inside a nucleon. Note, that the DA, Eq. (2.12), exhibits a flavour dependence due to the masses in the exponential. The exponential in (2.12) is merely introduced for theoretical purposes (e. g. in order to suppress the soft end-point regions). In the actual data fitting the exponential plays only a minor role. Therefore, the masses and the oscillator parameter are not considered as free parameters but taken from the literature. We stress that the constituent masses do not appear in the hard scattering amplitudes.

The dynamics of diquarks is governed by their coupling to gluons and photons. With respect to colour the diquark behaves like an antiquark. In order that the diquark in combination with a colour-triplet quark gives a colourless baryon it has to be in a colour antitriplet state. The colour part of the quark-diquark wave function (omitted in Eq. (2.2) is therefore $\psi^{\rm colour}_{\rm qD} = (1/\sqrt{3})\sum_{a=1}^{3}\delta_{a\bar{a}}$. The Feynman rules of electromagnetically interacting scalar diquarks are just those of standard scalar electrodynamics [32]. Replacement of the electric charge $e_0 e_{\rm S}$ by $-g_{\rm s}t^a$, with $g_{\rm s} = \sqrt{4\pi\alpha_{\rm s}}$ denoting the strong coupling constant and $t^a = \lambda^a/2$ Gell-Mann colour matrices, yields the corresponding Feynman rules for strongly interacting

scalar diquarks. The explicit expressions for γ-S and g-S vertices read:

$$\begin{aligned} &\mathrm{S}\gamma\mathrm{S}: \; -ie_0 e_\mathrm{S}(p_1+p_2)_\mu \; , \qquad \gamma\mathrm{SgS}: -2ie_0 e_\mathrm{S} g_\mathrm{s} t^a g_{\mu\nu} \; , \\ &\mathrm{SgS}: \quad ig_\mathrm{s} t^a (p_1+p_2)_\mu \; , \qquad \mathrm{gSgS}: ig_\mathrm{s}^2 \{t^a, t^b\} g_{\mu\nu} \; . \end{aligned} \tag{2.13}$$

During the calculation of Feynman diagrams diquarks are treated as point-like particles. The composite nature of diquarks is taken into account by multiplying the expressions for the various Feynman diagrams with diquark form factors

$$F_\mathrm{S}^{(n+2)}(Q^2) = \delta_\mathrm{S} \frac{Q_\mathrm{S}^2}{Q_\mathrm{S}^2 + Q^2} \begin{cases} 1 & n = 1 \\ a_\mathrm{S} & n \geq 2 \end{cases} \tag{2.14}$$

which depend on the number (n) of gauge bosons going to the diquark. This choice of the form factors ensures that the scaling behaviour of the diquark model goes over into that of the pure quark model in the limit $p_\perp \to \infty$. The factor $\delta_\mathrm{S} = \alpha_\mathrm{s}(Q^2)/\alpha_\mathrm{s}(Q_\mathrm{S}^2)$ ($\delta_\mathrm{S} = 1$ for $Q^2 \leq Q_\mathrm{S}^2$) provides the correct powers of $\alpha_\mathrm{s}(Q^2)$ for asymptotically large Q^2. For the running coupling constant α_s the one-loop result $\alpha_\mathrm{s} = 12\pi/25\ln(Q^2/\Lambda_\mathrm{QCD}^2)$ is used with $\Lambda_\mathrm{QCD} = 200$ MeV. In addition, α_s is restricted to be smaller than 0.5. The possibility of diquark excitation and break-up in intermediate states where diquarks can be far off-shell is taken into consideration by means of the strength parameter a_S.

Due to the reasons already mentioned, vector diquarks do not show up in the reactions we are investigating in the present paper. However, they have been dealt with in Refs. [20–22] to which we refer for further details of the diquark model.

III. PHOTOPRODUCTION OF MESONS – KINEMATICS AND HELICITY AMPLITUDES

Exclusive photoproduction of pseudoscalar mesons can, in general, be described by 4 independent helicity amplitudes. Following the notation of Ref. [33] we denote these amplitudes by

$$N = M_{0,-\frac{1}{2},+1,+\frac{1}{2}}\,, \qquad S_1 = M_{0,-\frac{1}{2},+1,-\frac{1}{2}}\,,$$
$$D = M_{0,+\frac{1}{2},+1,-\frac{1}{2}}\,, \qquad S_2 = M_{0,+\frac{1}{2},+1,+\frac{1}{2}}\,. \tag{3.1}$$

N , S_1, S_2, and D represent non-flip, single-flip, and double-flip amplitudes, respectively. Our helicity amplitudes are normalized in such a way that the unpolarized differential cross section is given by

$$\frac{d\sigma}{dt} = \frac{1}{32\pi(s-m_{\rm p}^2)^2}\left(|N|^2+|S_1|^2+|S_2|^2+|D|^2\right)\,. \tag{3.2}$$

As we have argued above two of the four amplitudes vanish, $N = D = 0$, if we concentrate on the particular process $\gamma{\rm p} \longrightarrow {\rm K}^+\Lambda$ and treat it within the diquark model. Out of the 15 polarization observables discussed in Ref. [33] there are only 3 observables which remain nonzero and which differ from each other (and from $d\sigma/dt$) for vanishing N and D. These can be chosen as the photon asymmetry

$$\Sigma\frac{d\sigma}{dt} = \frac{d\sigma_\perp}{dt} - \frac{d\sigma_\parallel}{dt} = \frac{1}{16\pi(s-m_{\rm p}^2)^2}\Re\left(S_1^* S_2 - N D^*\right)\,, \tag{3.3}$$

and the two double-polarization observables

$$G\frac{d\sigma}{dt} = -\frac{1}{16\pi(s-m_{\rm p}^2)^2}\Im\left(S_1 S_2^* + N D^*\right)\,, \tag{3.4}$$

and

$$E\frac{d\sigma}{dt} = \frac{1}{32\pi(s-m_{\rm p}^2)^2}\left(|N|^2-|S_1|^2+|S_2|^2-|D|^2\right)\,. \tag{3.5}$$

$d\sigma_\perp$ ($d\sigma_\parallel$) denotes the cross section for photons polarized perpendicular (parallel) to the reaction plane.

Photoproduction of vector mesons may be expressed by altogether 12 linear independent helicity amplitudes [34]. The diquark model leaves four amplitudes nonzero if applied to the formation of the ${\rm K}^{*+}$-Λ final state. In addition to S_1 and S_2 one can choose, e.g., $M_{+1,-\frac{1}{2},+1,+\frac{1}{2}}$ and $M_{-1,+\frac{1}{2},+1,-\frac{1}{2}}$. Due to the lack of experimental data we will restrict our discussion of ${\rm K}^{*+}$-Λ production to the unpolarized differential cross section which is obtained from Eq. (3.2) by including also $|M_{+1,-\frac{1}{2},+1,+\frac{1}{2}}|^2$ and $|M_{-1,+\frac{1}{2},+1,-\frac{1}{2}}|^2$.

The hard scattering amplitude $\widehat{T}_{\{\lambda\}}$ for the elementary process $\gamma \mathrm{uS}_{[\mathrm{u,s}]} \longrightarrow \mathrm{u\bar{s}sS}_{[\mathrm{u,s}]}$ consists, in general, of 79 different tree diagrams. However, only 63 diagrams are encountered if the outgoing meson is a K^+ or K^{*+}. The other 16 diagrams require the s-$\bar{\mathrm{s}}$ pair to go into the produced meson. Diagrams of this type would, e.g., be important in $\gamma \mathrm{p} \longrightarrow \phi \mathrm{p}$.

The helicity structure of the hard scattering amplitude $\widehat{T}_{\{\lambda\}}$ is particularly simple for the K^+-Λ and K^{*+}-Λ final states. Assigning helicity labels to the hadronic constituents as in Fig. 1 one finds (with the S diquark helicities $\lambda_2 = \lambda_6 = 0$):

$$\begin{aligned} \lambda_{\mathrm{p}} = \lambda_1 &= \quad \lambda_3 \,, \\ \lambda_\Lambda = \lambda_5 &= -\lambda_4 \,. \end{aligned} \tag{3.6}$$

Thus the quark helicities are uniquely determined by the proton and Λ helicity, respectively. The additional relation (hadronic helicity conservation)

$$\lambda_3 + \lambda_4 = \lambda_{\mathrm{p}} - \lambda_\Lambda = \lambda_{\mathrm{K}^{(*)}} \tag{3.7}$$

is the condition for the hard scattering amplitude $\widehat{T}_{\{\lambda\}}$ and consequently the hadronic amplitude $M_{\{\lambda\}}$ to become nonzero within the diquark model.

As depicted in Fig. 2 the hard scattering amplitude $\widehat{T}_{\{\lambda\}}(x_1, y_1, z_1; \hat{s}, \hat{t})$ for the elementary process $\gamma \mathrm{uS}_{[\mathrm{u,d}]} \longrightarrow \mathrm{u\bar{s}sS}_{[\mathrm{u,d}]}$ can be decomposed into 3-, 4-, and 5-point contributions

$$\begin{aligned} \widehat{T}_{\{\lambda\}}(x_1, y_1, z_1; \hat{s}, \hat{t}) = &-\frac{2}{\sqrt{6}} e_{\mathrm{u}} \ \left(\widehat{T}^{(3,\mathrm{q})}_{\{\lambda\}}(x_1, y_1, z_1; \hat{s}, \hat{t}) + \widehat{T}^{(4,\mathrm{q})}_{\{\lambda\}}(x_1, y_1, z_1; \hat{s}, \hat{t}) \right) \\ &-\frac{2}{\sqrt{6}} e_{\mathrm{s}} \ \left(\widehat{T}^{(3,\bar{\mathrm{q}})}_{\{\lambda\}}(x_1, y_1, z_1; \hat{s}, \hat{t}) + \widehat{T}^{(4,\bar{\mathrm{q}})}_{\{\lambda\}}(x_1, y_1, z_1; \hat{s}, \hat{t}) \right) \\ &-\frac{2}{\sqrt{6}} e_{\mathrm{ud}} \left(\widehat{T}^{(4,\mathrm{S})}_{\{\lambda\}}(x_1, y_1, z_1; \hat{s}, \hat{t}) + \widehat{T}^{(5,\mathrm{S})}_{\{\lambda\}}(x_1, y_1, z_1; \hat{s}, \hat{t}) \right) \,, \end{aligned} \tag{3.8}$$

depending on whether one, two, or three gauge bosons go to the diquark. The additional superscripts q, $\bar{\mathrm{q}}$, and S occurring in Eq. (3.8) indicate whether the photon couples to the u quark, the s quark, or the S diquark, respectively. For the numerical evaluation of the convolution integral Eq. (2.1) it is advantageous to further subdivide the various n-point contributions into two parts which differ by their propagator singularities:

$$
\begin{aligned}
\widehat{T}^{(3,\mathrm{q})}_{\{\lambda\}}(x_1,y_1,z_1;\hat{s},\hat{t}) &= \frac{f^{(3,\mathrm{q})}_{\{\lambda\}}(x_1,y_1,z_1;\hat{s},\hat{t})}{(q_2^2+i\epsilon)(g_1^2+i\epsilon')} + \frac{g^{(3,\mathrm{q})}_{\{\lambda\}}(x_1,y_1,z_1;\hat{s},\hat{t})}{(q_3^2+i\epsilon)(q_4^2+i\epsilon')}\,,\\
\widehat{T}^{(3,\bar{\mathrm{q}})}_{\{\lambda\}}(x_1,y_1,z_1;\hat{s},\hat{t}) &= \frac{f^{(3,\bar{\mathrm{q}})}_{\{\lambda\}}(x_1,y_1,z_1;\hat{s},\hat{t})}{(q_2^2+i\epsilon)(q_5^2+i\epsilon')} + \frac{g^{(3,\bar{\mathrm{q}})}_{\{\lambda\}}(x_1,y_1,z_1;\hat{s},\hat{t})}{(q_3^2+i\epsilon)(g_3^2+i\epsilon')}\,,\\
\widehat{T}^{(4,\mathrm{q})}_{\{\lambda\}}(x_1,y_1,z_1;\hat{s},\hat{t}) &= \frac{f^{(4,\mathrm{q})}_{\{\lambda\}}(x_1,y_1,z_1;\hat{s},\hat{t})}{(g_1^2+i\epsilon)(D_1^2+i\epsilon')} + \frac{g^{(4,\mathrm{q})}_{\{\lambda\}}(x_1,y_1,z_1;\hat{s},\hat{t})}{(g_1^2+i\epsilon)}\,,\\
\widehat{T}^{(4,\bar{\mathrm{q}})}_{\{\lambda\}}(x_1,y_1,z_1;\hat{s},\hat{t}) &= \frac{f^{(4,\bar{\mathrm{q}})}_{\{\lambda\}}(x_1,y_1,z_1;\hat{s},\hat{t})}{(g_3^2+i\epsilon)(D_2^2+i\epsilon')} + \frac{g^{(4,\bar{\mathrm{q}})}_{\{\lambda\}}(x_1,y_1,z_1;\hat{s},\hat{t})}{(g_3^2+i\epsilon)}\,,\\
\widehat{T}^{(4,\mathrm{S})}_{\{\lambda\}}(x_1,y_1,z_1;\hat{s},\hat{t}) &= \frac{f^{(4,\mathrm{S})}_{\{\lambda\}}(x_1,y_1,z_1;\hat{s},\hat{t})}{(q_5^2+i\epsilon)(g_2^2+i\epsilon')} + \frac{g^{(4,\mathrm{S})}_{\{\lambda\}}(x_1,y_1,z_1;\hat{s},\hat{t})}{(q_4^2+i\epsilon)(g_2^2+i\epsilon')}\,,\\
\widehat{T}^{(5,\mathrm{S})}_{\{\lambda\}}(x_1,y_1,z_1;\hat{s},\hat{t}) &= \frac{f^{(5,\mathrm{S})}_{\{\lambda\}}(x_1,y_1,z_1;\hat{s},\hat{t})}{(D_1^2+i\epsilon)(D_2^2+i\epsilon')} + \frac{g^{(5,\mathrm{S})}_{\{\lambda\}}(x_1,y_1,z_1;\hat{s},\hat{t})}{(g_2^2+i\epsilon)}\,.
\end{aligned}
\tag{3.9}
$$

Apart from g_3^{-2} the q_i^{-2}, D_i^{-2}, and g_i^{-2} denote just those quark, diquark, and gluon propagators which can go on-shell when integrating over x_1, y_1, and z_1. In order to make symmetry properties of the functions f and g with respect to interchange of Mandelstam variables and momentum fractions more obvious (cf. Appendix A) we have also extracted the non-singular gluon propagator g_3^{-2}. Explicitly the propagator denominators read:

$$
\begin{aligned}
q_2^2 &= y_2z_2\hat{s} + x_2y_2\hat{t} + x_2z_2\hat{u}\,, & g_1^2 &= z_2\hat{s} + x_2\hat{t} + x_2z_2\hat{u}\,,\\
q_3^2 &= y_2z_1\hat{s} + x_2y_2\hat{t} + x_2z_1\hat{u}\,, & g_2^2 &= y_1\hat{s} + x_1y_1\hat{t} + x_1\hat{u}\,,\\
q_4^2 &= y_1z_2\hat{s} + x_1y_1\hat{t} + x_1z_2\hat{u}\,, & g_3^2 &= y_2z_1\hat{s} + y_2\hat{t} + z_1\hat{u}\,,\\
q_5^2 &= y_1z_1\hat{s} + x_1y_1\hat{t} + x_1z_1\hat{u}\,, & D_1^2 &= y_1z_2\hat{s} + x_2y_1\hat{t} + x_2z_2\hat{u}\,,\\
& & D_2^2 &= y_2z_1\hat{s} + x_1y_2\hat{t} + x_1z_1\hat{u}\,.
\end{aligned}
\tag{3.10}
$$

As already indicated in Eq. (3.9) propagator singularities are treated by means of the usual $i\epsilon$ prescription.

Analytical expressions for the functions f and g (cf. Appendix A) have been derived with the help of "FeynArts" [35] and "FeynCalc" [36] – two program packages written in "Mathematica "which serve the automatic generation and evaluation of Feynman diagrams. Since "FeynArts" only contains the Feynman rules of the Standard Model it had to be extended to deal with S diquarks as well. The spinor techniques developed by Kleiss and Stirling [37]

have been utilized to convert strings of gamma matrices sandwiched between spinors into traces which can be handled by "FeynCalc". A strong indication for the correctness of our results is already the agreement (apart from a detected sign error) with a previous independent calculation [38] performed with "FORM" [39] (another symbolic computer program for high-energy physics). Further checks of our analytical results were carried out by testing the U(1) gauge invariance with respect to the photon and the SU(3) gauge invariance with respect to the gluon. The proof of gauge invariance is facilitated by observing that not only the sum of all 63 tree diagrams gives a gauge invariant expression, but rather each of the functions f and g in Eq. (3.9) is by itself gauge invariant. In addition to the gauge invariance tests a few diagrams were recalculated by hand.

IV. NUMERICAL RESULTS

Our numerical studies are performed with the set of diquark-model parameters

$$f_{\rm S} = 73.85\,{\rm MeV}, \quad Q_{\rm S}^2 = 3.22\,{\rm GeV}^2, \quad a_{\rm S} = 0.15\;, \tag{4.1}$$

which has been found by fitting elastic electron-nucleon scattering data [20] and which provides also reasonable results in other applications of the diquark model [21,22]. A detailed explanation how the convolution integral, Eq. (2.1), for the various n-point contributions has been treated numerically is given in Appendix B. At this point we only want to emphasize that propagator singularities have been carefully separated and integrated analytically. The remaining integrals could be performed by means of rather fast fixed-point Gaussian quadrature.

One of the characteristic qualitative features of perturbative QCD predictions is the fixed-angle scaling behaviour of cross sections. Within the diquark model the $\gamma{\rm p} \longrightarrow {\rm K}^{(*)^+}\Lambda$ cross section behaves at large $\hat{s}$ like

$$\frac{d\sigma}{dt} \propto \hat{s}^{-5} \left[F_{\rm S}^{(3)}(- < x_2 >< y_2 > \hat{t})\right]^2 h(\hat{t}/\hat{s}) \stackrel{\hat{s}\to\infty}{\longrightarrow} \hat{s}^{-7}\tilde{h}(\hat{t}/\hat{s})\,. \tag{4.2}$$

$< x_2 >$ and $< y_2 >$ denote average values of the longitudinal momentum fraction of the diquark in a proton or Λ, respectively. Equation (4.2) shows that the scaling behaviour of the pure quark hard-scattering model [10] is recovered in the limit $\hat{s} \to \infty$. However, at finite $\hat{s}$, where the diquark form factor $F_{\rm S}^{(3)}$ becomes operational and diquarks appear as nearly elementary particles, the $\hat{s}^{-7}$ power-law is modified. Additional deviations from the $\hat{s}^{-7}$ decay of the cross section are due to logarithmic corrections (hidden in the functions $F_{\rm S}^{(3)}$ and h) which have there origin in the running coupling constant $\alpha_{\rm s}$ and eventually in the evolution of the DAs ϕ (neglected in our calculation).

A. $\gamma \mathbf{p} \longrightarrow \mathbf{K}^+ \Lambda$

Figure 3 shows the diquark-model predictions for $s^7 d\sigma/dt$ along with the few existing large-momentum transfer data [40] and the outcome of the pure quark hard-scattering model [19] (long-dashed curve). Whereas the DAs of proton and Λ have been kept fixed according to Eq. (2.12) we have varied the K^+ DA. The solid and the short-dashed line represent results for the asymptotic (Eq. (2.8)) and the two-humped (Eq. (2.9)) K^+ DA, respectively, evaluated at $E_{\rm lab}^{\gamma} = 6$ GeV. The better performance of the asymptotic DA and the overshooting of the asymmetric DA is in line with the conclusion drawn from the investigation of the pion-photon transition form factor [15,41] where, for the case of the pion, the CZ DA is clearly ruled out. There, strongly end-point concentrated DAs are also overshooting the data. Our findings have to be contrasted with those obtained within the pure quark-model calculation of photoproduction [19], where the asymptotic forms for both, baryon and meson DAs, give systematically larger results than the combination of very asymmetric DAs. However, the numerics of Ref. [19] must be taken with some provisio. For Compton scattering off nucleons it has been demonstrated [42] that the very crude treatment of propagator singularities adopted in Ref. [19], namely keeping $i\epsilon$ small but finite, may lead to deviations from the correct result which are as large as one order of magnitude. The sensitivity of our calculation to the choice of the baryon DAs has been checked only with respect to their end-point

behaviour $x \to 0, 1$. Neglecting the exponential factor in Eq. (2.12) results in a slight reduction of the cross section, e.g. $\approx 8\%$ at $\theta_{\rm cm} = 90^\circ$ and $E^\gamma_{\rm lab} = 6$ GeV. Deviations from the scaling behaviour can be estimated by comparing the dash-double-dotted and the solid curve, which correspond to the asymptotic K^+ DA at $E^\gamma_{\rm lab} = 4$ and 6 GeV, respectively.

We have also examined the relative importance of various groups of Feynman graphs and found the 3-point contributions to be by far the most important. 4- and 5-point contributions amount to $\approx 5\%$ at $\theta_{\rm cm} = 90^\circ$ and $E^\gamma_{\rm lab} = 6$ GeV as long as only $d\sigma/dt$ is considered. Their influence decreases from larger to smaller angles. Spin observables, on the other hand, are much more affected by 4- and 5-point contributions.

The three non-vanishing spin observables E, Σ, and G are depicted in Fig. 4. Whereas E measures the relative strength of the two amplitudes S_1 and S_2, Σ and G are in addition influenced by the phase difference of these two amplitudes. To make the interplay of the two amplitudes S_1 and S_2 more obvious we have also plotted their moduli and phases in Figs. 5 and 6, respectively. For both choices of the Kaon DA S_1 is observed to be the dominant amplitude in backward direction. For $\phi^{\rm K}_{\rm CZ}$ it remains dominant over the whole angular range. In contrast, S_2 becomes increasingly important for $\phi^{\rm K}_{\rm asy}$ if one goes from backward to forward direction. This behaviour is clearly reflected by the double-polarization observable E. The phase difference between S_1 and S_2 varies rather moderately over the whole angular range for $\phi^{\rm K}_{\rm asy}$, whereas it changes dramatically for $\phi^{\rm K}_{\rm CZ}$. Unfortunately, the information on the phase difference is hidden in the photon asymmetry Σ and the double polarization observable G for which the dependence on the choice of the Kaon DA is not so aggravating.

Let us recall at this point that the occurrence of nontrivial phases in photoproduction amplitudes is a consequence of the fact that most of the Feynman diagrams contain internal gluons that can propagate on mass shell in certain kinematic regions of the momentum-fraction space. The treatment of the corresponding propagator singularities by means of the usual Feynman prescription results in an imaginary contribution to photoproduction amplitudes. One may worry about the validity of perturbation theory for a freely propagating gluon which is expected to be modified by long-distance effects. But fortunately photopro-

duction belongs to a class of exclusive reactions which does, to leading order perturbative QCD, not require the resummation of gluonic radiative corrections (Sudakov effects). As has been proved in Ref. [43] the standard factorization formula, Eq. (2.1), produces already an infrared finite amplitude.

Unlike Σ, G, and E, which have not been measured as yet, the determination of the Λ polarization P has been attempted already [44] (for more recent efforts, cf. Ref. [6]). The way to determine the transverse polarization of the Λ is to detect, in addition to the K^+, the proton coming from the weak $\Lambda \longrightarrow p\pi^-$ decay. The transverse Λ polarization P then follows from the known (P dependent) angular distribution of the weak $\Lambda \longrightarrow p\pi^-$ decay. According to the diquark model, and also the pure quark model, P is expected to vanish in the hard-scattering regime ($tu/s \gg m_p^2$). The present data, however, are at too small s and t to allow conclusions about the validity and quality of these perturbative models. It would be interesting to see, whether the occurrence of sizable transverse polarizations at $p_\perp \approx$ few GeV, as observed e.g. in elastic p-p scattering [45] or inclusive production of hyperons in p-p collisions [46], continues to the $\gamma p \longrightarrow K^+\Lambda$ process. This would be an indication that, besides the perturbative mechanism, non-perturbative physics (beyond diquarks) is still at work.

We have also computed differential cross sections for the reaction $\gamma n \longrightarrow K^0\Lambda$. For $\cos(\theta_{cm}) \geq 0$ they are considerably smaller than the corresponding $\gamma p \longrightarrow K^+\Lambda$ cross sections. The amount of suppression depends on the choice of the K^0 DA. For the asymptotic DA the suppression factor is ≈ 10 in the whole forward region, whereas it increases for the two-humped DA from 2 to ≈ 10 when $\cos(\theta_{cm})$ is varied from 0 to 0.8 ($E^\gamma_{lab} = 6$ GeV). In view of the plans at CEBAF to study $\gamma n \longrightarrow K^0\Lambda$ by means of a deuteron target [5] this is certainly an interesting observation which could be helpful to pin down the uncertainties of the Kaon DA.

B. $\gamma p \longrightarrow K^{*+}\Lambda$

The diquark-model results for $(d\sigma/dt)_{\gamma p \to K^{*+}\Lambda}$ are plotted in Fig. 7. Again curves are shown for two choices of the K^{*+} DA with p and Λ DA kept fixed ($E^{\gamma}_{\rm lab} = 6$ GeV). The results resemble those for photoproduction of K^+ mesons. Cross sections for the asymmetric DA, Eqs. (2.10) and (2.11), are nearly one order of magnitude larger than for the asymptotic DA, Eq. (2.8). If $\phi_{\rm asy}$ is taken for both, K^+ and K^{*+}, the photoproduction cross section for the K^{*+} vector meson is found to be by a factor of 1.8 - 3.6 (depending on the scattering angle) larger than that for the pseudoscalar K^+ meson. An increase by a factor 1.73 is due to the different K^+ and K^{*+} decay constants $f^{\rm K}$ and $f^{\rm K^*}$. The remaining difference is caused by the contribution of transversially polarized K^{*+} mesons, which increases from small to large scattering angles. The situation would be quite similar if we had taken $\phi^{\rm K}_{\rm CZ}$ for both, K^+ and K^{*+}. However, the enhancement of the K^{*+} cross section is completely compensated, if $\phi^{\rm K}_{\rm CZ}$ is replaced by $\phi^{\rm K^*}_{\rm L}$ and $\phi^{\rm K^*}_{\rm T}$ (cf. Eqs. (2.10) and (2.11)) when going from K^+ to K^{*+} photoproduction.

Till now large momentum transfer data for photoproduction of vector mesons are only available for the reaction $\gamma p \longrightarrow (\rho_0 + \omega)p$ [40]. At $\theta_{\rm cm} = 90^\circ$ and $E^{\gamma}_{\rm lab} \approx 6$ GeV the experimental value of the cross section ratio $(d\sigma/dt)_{\gamma p \to (\rho_0+\omega)p}/(d\sigma/dt)_{\gamma p \to \pi_0 p}$ is ≈ 2. This means in particular that $(d\sigma/dt)_{\gamma p \to \rho_0 p} \lesssim 2(d\sigma/dt)_{\gamma p \to \pi_0 p}$. The difference in the ρ_0 and π_0 decay constants ($f^{\rho}_{\rm decay} \approx 1.5 f^{\pi}_{\rm decay}$), however, already implies an enhancement of the ρ_0 photoproduction cross section as compared to the π_0 one by a factor of ≈ 2.3 which is further magnified by contributions of transversially polarized ρs. The only way to compensate part of this enhancement is to assume that (as above in the case of K^+ and K^{*+}) the DAs of π and ρ differ from each other. Experimental data on photoproduction of pseudoscalar and vector mesons with the same flavour content could thus be very useful to work out differences in the corresponding DAs.

V. SUMMARY AND CONCLUSIONS

We have investigated photoproduction of K-Λ and K*-Λ final states in the few-GeV momentum-transfer region. Our analysis is based on perturbative QCD supplemented by the assumption that baryons can be treated as quark-diquark systems. The present calculation continues previous work on photon-induced hadronic reactions [20–22] performed within the same approach. By modeling quark-quark correlations inside a baryon as quasi-elementary particles - scalar and vector diquarks - we account for some non-perturbative effects. In this way we are able to extend the range of applicability of the pure quark hard-scattering approach from large down to moderately large momentum transfers. The fact that the photoproduction channels we are interested in contain a Λ in the final state entails a considerable reduction in computational effort. In contrast to arbitrary photoproduction reactions only scalar diquarks must be taken into consideration. This has the consequence that helicity amplitudes and hence spin-observables violating hadronic helicity conservation (cf. Eq. (3.7)), e.g. the Λ polarization, are predicted to vanish.

Our numerical studies have been performed with the diquark-model parameters and the quark-diquark DAs proposed in Ref. [20]. We have paid special attention to the correct and numerically robust treatment of propagator singularities (cf. Appendix B). Reasonable agreement with the few existing $\gamma p \longrightarrow K^+\Lambda$ data is achieved already with the asymptotic form for the K^+ DA. On the other hand, the end-point concentrated K^+ DA, based on QCD sum rules [11], seems to perform less well. The corresponding curve lies far beyond the data. The difference between these two Kaon DAs is also clearly visible in the three non-vanishing polarization observables, i.e. the photon asymmetry Σ and the two double-polarization observables G and E. It is most pronounced in the observable E. Another quantity which we found to be very sensitive on the choice of the Kaon DA is the angular dependence of the cross-section ratio $(d\sigma/dt)_{\gamma n\to K^0\Lambda}/(d\sigma/dt)_{\gamma p\to K^+\Lambda}$. For the photoproduction of the K* vector meson there are no data to compare with. We have again tested the asymptotic DA and a K* DA which obeys QCD sum-rule constraints on the lowest moments [29]. The

differences in the results for the two DAs are quite similar to those for photoproduction of the pseudoscalar K^+ meson. When going from K to K^* photoproduction the cross section becomes larger due to the different K and K^* decay constants and the additional contributions from transversially polarized K^*s. This increase of the cross section, however, is partly compensated if different DAs for K and K^* are used.

With regard to future experiments we consider, apart from more and better large $p_\perp$ cross section data, the polarization measurement of the recoiling Λ as one of the most urgent tasks. A large polarization indicates that the perturbative QCD regime has not been entered yet. In the perturbative QCD regime the Kaon DAs could be restricted by means of quantities, like the photon asymmetry or the cross section ratios $(d\sigma/dt)_{\gamma n\to K^0\Lambda}/(d\sigma/dt)_{\gamma p\to K^+\Lambda}$ and $(d\sigma/dt)_{\gamma p\to K^{*+}\Lambda}/(d\sigma/dt)_{\gamma p\to K^+\Lambda}$, which are very sensitive to the choice of the DAs. With a maximal photon laboratory energy of (at present) 4 GeV CEBAF [5] touches at best the border of the hard-scattering domain. More decisive data could be expected from a future electron facility like ELFE [47] which is designed to explore the energy range up to 15 GeV (or even higher) with a continuous high intensity electron beam.

APPENDIX A: ANALYTICAL EXPRESSIONS FOR THE HARD AMPLITUDES

In this appendix we quote analytical expressions for those hard amplitudes which describe the process $\gamma uS(ud) \longrightarrow u\bar{s}sS(ud)$ with the $s\bar{s}$-pair being in a spin-zero state. More generally speaking, these are just the scalar diquark contributions to photoproduction of pseudoscalar mesons. According to Eq. (3.9) the various n-point contributions to these amplitudes can be decomposed into gauge invariant functions f and g. The functions f and g which determine the hadronic (helicity conserving) amplitude S_1 read

$$f^{(3,q)}_{0,-\frac{1}{2},+1,-\frac{1}{2}} = -C_F^{(1)} A_T^{(S,3)} \frac{z_2\hat{u}}{y_2 z_1 \hat{t}^2}\left[y_2\hat{t} + z_2\hat{u}\right] ,$$

$$g^{(3,q)}_{0,-\frac{1}{2},+1,-\frac{1}{2}} = -C_F^{(1)} A_T^{(S,3)} \frac{\hat{u}}{x_2 y_1 z_1 \hat{s}\hat{t}^2}\left[q_4^2(z_1\hat{s} + x_2\hat{t}) - x_2(x_2 - z_1)\hat{s}\hat{t}\right] ,$$

$$
\begin{aligned}
f^{(3,\bar{\mathrm{q}})}_{0,-\frac{1}{2},+1,-\frac{1}{2}} &= -C_{\mathrm{F}}^{(1)} A_{\mathrm{T}}^{(\mathrm{S},3)} \frac{1}{x_1 x_2 y_1 y_2 z_1 \hat{t}^2 \hat{u}} \Big[y_1 y_2^2 z_2 (x_2 - z_2) \hat{t}^3 \\
&\quad + y_2 ((y_1 - x_1)(y_1 z_2 + y_2 z_1) z_2 + (x_1 y_1 - z_1^2) x_2 y_1) \hat{t}^2 \hat{u} \\
&\quad + ((y_1 - x_1)(y_2^2 z_1 - x_2 y_1^2) z_2 + (y_1 z_2 - x_2 z_1) x_2 y_1 y_2) \hat{t} \hat{u}^2 \\
&\quad + x_2 y_1 (y_2 - x_2) z_1 z_2 \hat{u}^3 \Big] \,, \\
g^{(3,\bar{\mathrm{q}})}_{0,-\frac{1}{2},+1,-\frac{1}{2}} &= -C_{\mathrm{F}}^{(1)} A_{\mathrm{T}}^{(\mathrm{S},3)} \frac{\hat{s}}{x_2 y_1 \hat{t}^2} \Big[(x_2 - z_1) y_2 \hat{t} + y_1 z_1 \hat{u} \Big] \,, \\
f^{(4,\mathrm{q})}_{0,-\frac{1}{2},+1,-\frac{1}{2}} &= -C_{\mathrm{F}}^{(1)} A_{\mathrm{T}}^{(\mathrm{S},4)} \frac{\hat{u}}{y_1 z_1 \hat{s} \hat{t}} \Big[x_2 y_2 \hat{t} - D_1^2 \Big] \,, \\
g^{(4,\mathrm{q})}_{0,-\frac{1}{2},+1,-\frac{1}{2}} &= -C_{\mathrm{F}}^{(2)} A_{\mathrm{T}}^{(\mathrm{S},4)} \frac{\hat{u}}{x_2 y_1 y_2 z_1 \hat{s} \hat{t}^2} \Big[y_2 z_2 \hat{s} - x_2 \hat{t} - x_2 z_2 \hat{u} \Big] \,, \\
f^{(4,\bar{\mathrm{q}})}_{0,-\frac{1}{2},+1,-\frac{1}{2}} &= -C_{\mathrm{F}}^{(1)} A_{\mathrm{T}}^{(\mathrm{S},4)} \frac{1}{x_1 y_1 z_1 \hat{t} \hat{u}} \Big[\hat{s} \hat{t} x_2 y_2^2 + D_2^2 (y_2 \hat{t} - y_1 \hat{u})) \Big] \,, \\
g^{(4,\bar{\mathrm{q}})}_{0,-\frac{1}{2},+1,-\frac{1}{2}} &= C_{\mathrm{F}}^{(2)} A_{\mathrm{T}}^{(\mathrm{S},4)} \frac{1}{x_1 x_2 y_1 y_2 \hat{t}^2} \Big[g_3^2 (y_2 \hat{s} + x_2 \hat{u}) + x_1 y_2 \hat{t} \hat{u} \Big] \,, \\
f^{(4,\mathrm{S})}_{0,-\frac{1}{2},+1,-\frac{1}{2}} &= -C_{\mathrm{F}}^{(1)} A_{\mathrm{T}}^{(\mathrm{S},4)} \frac{y_1 z_2 \hat{s}}{x_1 z_1 \hat{u}} \\
g^{(4,\mathrm{S})}_{0,-\frac{1}{2},+1,-\frac{1}{2}} &= -C_{\mathrm{F}}^{(1)} A_{\mathrm{T}}^{(\mathrm{S},4)} \frac{1}{z_2 \hat{s}} \Big[x_1 \hat{t} + z_2 \hat{s} \Big] \,, \\
f^{(\bar{5},\mathrm{S})}_{0,-\frac{1}{2},+1,-\frac{1}{2}} &= -C_{\mathrm{F}}^{(1)} A_{\mathrm{T}}^{(\mathrm{S},5)} \frac{y_1 z_2 \hat{s}}{x_1 z_1 \hat{u}} \Big[(D_1^2 + x_2 y_1 \hat{t})(D_2^2 - y_2 \hat{u}) + x_2 y_2 (y_1 - y_2 + z_1) \hat{t} \hat{u} \Big] \,, \\
g^{(\bar{5},\mathrm{S})}_{0,-\frac{1}{2},+1,-\frac{1}{2}} &= -C_{\mathrm{F}}^{(2)} A_{\mathrm{T}}^{(\mathrm{S},5)} \frac{1}{x_1 y_1 z_1 z_2 \hat{s} \hat{u}} \left[x_1 \hat{u} + z_2 (x_1 \hat{u} - y_1 \hat{s}) \right] \,,
\end{aligned}
\tag{A1}
$$

with

$$
C_{\mathrm{F}}^{(1)} = \frac{16}{9\sqrt{3}} \,, \qquad C_{\mathrm{F}}^{(2)} = \frac{1}{\sqrt{3}} \,,
\tag{A2}
$$

and

$$
A_{\mathrm{T}}^{(\mathrm{S},n)} = 128 \pi^2 \sqrt{\pi \alpha} \alpha_{\mathrm{s}}^2 (\hat{t} \hat{u} / \hat{s}) \sqrt{-\hat{t}}\, F_{\mathrm{S}}^{(n)} (-x_2 y_2 t) \,,
\tag{A3}
$$

where α denotes the fine-structure constant.

The functions f and g contributing to the hadronic amplitude S_2 are obtained from those entering S_1 by interchange of the Mandelstam variables $\hat{s} \leftrightarrow \hat{u}$ and the momentum fractions $x_1 \leftrightarrow y_1$ and $z_1 \leftrightarrow z_2$. One finds in particular

$$
\begin{aligned}
f^{(3,\mathrm{q})}_{0,+\frac{1}{2},+1,+\frac{1}{2}} &= -g^{(3,\bar{\mathrm{q}})}_{0,-\frac{1}{2},+1,-\frac{1}{2}}(\hat{s}\leftrightarrow\hat{u}, x_1\leftrightarrow y_1, z_1\leftrightarrow z_2)\,,\\
g^{(3,\mathrm{q})}_{0,+\frac{1}{2},+1,+\frac{1}{2}} &= -f^{(3,\bar{\mathrm{q}})}_{0,-\frac{1}{2},+1,-\frac{1}{2}}(\hat{s}\leftrightarrow\hat{u}, x_1\leftrightarrow y_1, z_1\leftrightarrow z_2)\,,\\
f^{(3,\bar{\mathrm{q}})}_{0,+\frac{1}{2},+1,+\frac{1}{2}} &= -g^{(3,\mathrm{q})}_{0,-\frac{1}{2},+1,-\frac{1}{2}}(\hat{s}\leftrightarrow\hat{u}, x_1\leftrightarrow y_1, z_1\leftrightarrow z_2)\,,\\
g^{(3,\bar{\mathrm{q}})}_{0,+\frac{1}{2},+1,+\frac{1}{2}} &= -f^{(3,\mathrm{q})}_{0,-\frac{1}{2},+1,-\frac{1}{2}}(\hat{s}\leftrightarrow\hat{u}, x_1\leftrightarrow y_1, z_1\leftrightarrow z_2)\,,\\
f^{(4,\mathrm{q})}_{0,+\frac{1}{2},+1,+\frac{1}{2}} &= -f^{(4,\bar{\mathrm{q}})}_{0,-\frac{1}{2},+1,-\frac{1}{2}}(\hat{s}\leftrightarrow\hat{u}, x_1\leftrightarrow y_1, z_1\leftrightarrow z_2)\,,\\
g^{(4,\mathrm{q})}_{0,+\frac{1}{2},+1,+\frac{1}{2}} &= -g^{(4,\bar{\mathrm{q}})}_{0,-\frac{1}{2},+1,-\frac{1}{2}}(\hat{s}\leftrightarrow\hat{u}, x_1\leftrightarrow y_1, z_1\leftrightarrow z_2)\,,\\
f^{(4,\bar{\mathrm{q}})}_{0,+\frac{1}{2},+1,+\frac{1}{2}} &= -f^{(4,\mathrm{q})}_{0,-\frac{1}{2},+1,-\frac{1}{2}}(\hat{s}\leftrightarrow\hat{u}, x_1\leftrightarrow y_1, z_1\leftrightarrow z_2)\,,\\
g^{(4,\bar{\mathrm{q}})}_{0,+\frac{1}{2},+1,+\frac{1}{2}} &= -g^{(4,\mathrm{q})}_{0,-\frac{1}{2},+1,-\frac{1}{2}}(\hat{s}\leftrightarrow\hat{u}, x_1\leftrightarrow y_1, z_1\leftrightarrow z_2)\,,\\
f^{(4,\mathrm{S})}_{0,+\frac{1}{2},+1,+\frac{1}{2}} &= -g^{(4,\mathrm{S})}_{0,-\frac{1}{2},+1,-\frac{1}{2}}(\hat{s}\leftrightarrow\hat{u}, x_1\leftrightarrow y_1, z_1\leftrightarrow z_2)\,,\\
g^{(4,\mathrm{S})}_{0,+\frac{1}{2},+1,+\frac{1}{2}} &= -f^{(4,\mathrm{S})}_{0,-\frac{1}{2},+1,-\frac{1}{2}}(\hat{s}\leftrightarrow\hat{u}, x_1\leftrightarrow y_1, z_1\leftrightarrow z_2)\,,\\
f^{(5,\mathrm{S})}_{0,+\frac{1}{2},+1,+\frac{1}{2}} &= -f^{(5,\mathrm{S})}_{0,-\frac{1}{2},+1,-\frac{1}{2}}(\hat{s}\leftrightarrow\hat{u}, x_1\leftrightarrow y_1, z_1\leftrightarrow z_2)\,,\\
g^{(5,\mathrm{S})}_{0,+\frac{1}{2},+1,+\frac{1}{2}} &= -g^{(5,\mathrm{S})}_{0,-\frac{1}{2},+1,-\frac{1}{2}}(\hat{s}\leftrightarrow\hat{u}, x_1\leftrightarrow y_1, z_1\leftrightarrow z_2)\,.
\end{aligned}
\tag{A4}
$$

The hard amplitudes for photoproduction of longitudinally polarized K*-mesons are (up to a sign change in $\hat{T}_{0,-\frac{1}{2},+1,-\frac{1}{2}}$) also determined by these expressions. For photoproduction of transversially polarized K*-mesons the functions f and g are of similar length and shape and can be obtained from the authors on request.

APPENDIX B: NUMERICAL TREATMENT OF PROPAGATOR POLES

The numerical difficulties in performing the convolution integral Eq. (2.1) are mainly caused by the occurrence of propagator singularities in the range of integration which give rise to a principal value integral

$$
\frac{1}{k^2+i\epsilon} = \wp\left(\frac{1}{k^2}\right) - i\pi\delta(k^2)\,. \tag{B1}
$$

In what follows, the four cases to be distinguished will be discussed separately.

1. No propagator on shell

The only contribution to the convolution integral Eq. (2.1) exhibiting no propagator singularity is the one corresponding to $g^{(4,\bar{\mathrm{q}})}_{\{\lambda\}}$ (cf. Eq. (3.9)). In these circumstances the convolution integral is easily performed by means of 3-dimensional Gaussian quadrature.

2. One propagator on shell

If only one of the propagators goes on shell within the integration region – this happens for $g^{(3,\bar{\mathrm{q}})}_{\{\lambda\}}$, $g^{(4,\mathrm{q})}_{\{\lambda\}}$, $f^{(4,\bar{\mathrm{q}})}_{\{\lambda\}}$, and $g^{(5,\mathrm{S})}_{\{\lambda\}}$ – the corresponding integrals over x_1 have the general structure:

$$I^{(k)}(y_1,z_1)=\int_0^1 dx_1 \frac{h(x_1,y_1,z_1)}{k^2+i\epsilon}\,. \tag{B2}$$

In order to simplify notations we have neglected helicity labels and the dependence on the Mandelstam variables $\hat{s}$ and $\hat{t}$. Furthermore, the distribution amplitudes $\phi_{\mathrm{p}}(x_1)$, $\phi^{\dagger}_{\Lambda}(y_1)$, and $\phi^{\dagger}_{\mathrm{K}}(z_1)$ have been absorbed into the function $h(x_1,y_1,z_1)$. The integral $I^{(k)}$ may be rewritten to give

$$\begin{aligned} I^{(k)}(y_1,z_1)=&\int_0^1 dx_1 \frac{h(x_1,y_1,z_1)-h(x_1^{(k)},y_1,z_1)}{k^2} \\ &+h(x_1^{(k)},y_1,z_1)\left(\wp\int_0^1\frac{dx_1}{k^2}-i\pi\left|\frac{\partial k^2}{\partial x_1}\right|^{-1}\right)\,, \end{aligned} \tag{B3}$$

where $x_1^{(k)}=x_1^{(k)}(y_1,z_1)$ represents the zero of k^2 (considered as a function of x_1). The first integral in Eq. (B3) is now again tractable by simple Gaussian quadrature, whereas the principal-value integral can be done analytically. Since $I^{(k)}$ is a regular function of y_1 and z_1 Gaussian integration can also be applied to these variables. Analytical expressions for propagator-pole positions, principal value integrals and x_1-derivatives of propagator denominators are listed in Table I.

3. Two propagators on shell – propagator poles not coinciding

If two propagators k_1^{-2} and k_2^{-2} go on shell one can proceed similarly as in the one-pole case, provided the zeroes $x_1^{(k_1)} = x_1^{(k_1)}(y_1, z_1)$ and $x_1^{(k_2)} = x_1^{(k_2)}(y_1, z_1)$ of k_1^2 and k_2^2 (considered as functions of x_1) do not coincide for fixed y_1 and z_1, $0 < y_1, z_1 < 1$ arbitrary. This is guaranteed for the Feynman diagrams contributing to $f_{\{\lambda\}}^{(3,\mathrm{q})}$, $f_{\{\lambda\}}^{(4,\mathrm{q})}$, $f_{\{\lambda\}}^{(4,\mathrm{S})}$, and $g_{\{\lambda\}}^{(4,\mathrm{S})}$. The x_1-integrals to be considered have the general form

$$I^{(k_1,k_2)}(y_1, z_1) = \int_0^1 dx_1 \frac{h(x_1, y_1, z_1)}{(k_1^2 + i\epsilon)(k_2^2 + i\epsilon')} \,. \tag{B4}$$

If $x_1^{(k_1)} \neq x_1^{(k_2)}$ a partial fractioning yields

$$I^{(k_1,k_2)}(y_1, z_1) = \frac{1}{x_1^{(k_1)} - x_1^{(k_2)}} \left\{ \left(\frac{\partial k_2^2}{\partial x_1} \right)^{-1} I^{(k_1)}(y_1, z_1) - \left(\frac{\partial k_1^2}{\partial x_1} \right)^{-1} I^{(k_2)}(y_1, z_1) \right\} , \tag{B5}$$

i.e., two terms which again can be treated according to Eq. (B3).

4. Two propagators on shell – propagator poles coinciding

This is the worst case and shows up in connection with the functions $g_{\{\lambda\}}^{(3,\mathrm{q})}$, $f_{\{\lambda\}}^{(3,\bar{\mathrm{q}})}$, and $f_{\{\lambda\}}^{(5,\mathrm{S})}$. The general structure of the x_1-integrals is again that of Eq. (B4). However, now it happens that the two propagator singularities $x_1^{(k_1)}$ and $x_1^{(k_2)}$ (which still depend on y_1 and z_1) coincide for a certain value of y_1 ($0 < y_1 < 1$), $0 < z_1 < 1$ fixed. We denote this value by $y_1^{(k_1,k_2)} = y_1^{(k_1,k_2)}(z_1)$ – it still depends on z_1. We note that the partial fractioning can still be performed for arbitrary values of y_1 and z_1 as long as ϵ and ϵ' are kept finite. By carefully taking the limit $\epsilon \to 0$ in the terms containing k_1^2 and $\epsilon' \to 0$ in the terms containing k_2^2 and using Eq. (B3) one ends up with

$$
\begin{aligned}
I^{(k_1,k_2)}(y_1,z_1) = \frac{1}{x_1^{(k_1)} - x_1^{(k_2)} + i\tilde{\epsilon}} \Bigg\{ & \left(\frac{\partial k_2^2}{\partial x_1}\right)^{-1} \int_0^1 dx_1 \frac{h(x_1,y_1,z_1) - h(x_1^{(k_1)},y_1,z_1)}{k_1^2} \\
& + \left(\frac{\partial k_2^2}{\partial x_1}\right)^{-1} h(x_1^{(k_1)},y_1,z_1) \left(\wp \int_0^1 \frac{dx_1}{k_1^2} - i\pi \left| \frac{\partial k_1^2}{\partial x_1} \right|^{-1} \right) \\
& - \left(\frac{\partial k_1^2}{\partial x_1}\right)^{-1} \int_0^1 dx_1 \frac{h(x_1,y_1,z_1) - h(x_1^{(k_2)},y_1,z_1)}{k_2^2} \\
& - \left(\frac{\partial k_1^2}{\partial x_1}\right)^{-1} h(x_1^{(k_2)},y_1,z_1) \left(\wp \int_0^1 \frac{dx_1}{k_2^2} - i\pi \left| \frac{\partial k_2^2}{\partial x_1} \right|^{-1} \right) \Bigg\} .
\end{aligned}
\tag{B6}
$$

In Eq. (B6) $\tilde{\epsilon}$ stands for either ϵ or ϵ'. Closer inspection of $(x_1^{(k_1)} - x_1^{(k_2)})$ (considered as function of y_1) reveals that the zero $y_1^{(k_1,k_2)}$ is quadratic. On the other hand one also finds that $y_1^{(k_1,k_2)}$ is a single zero of both $h(x_1^{(k_1)},y_1,z_1)$ and $h(x_1^{(k_2)},y_1,z_1)$. This immediately implies that the real part of $I^{(k_1,k_2)}(y_1,z_1)$ is a regular function of y_1 and also z_1 so that Gaussian quadrature is again applicable to the corresponding integrations. Taking further into account that $(\partial k_1^2/\partial x_1)^{-1}$ and $(\partial k_2^2/\partial x_1)^{-1}$ have different signs the imaginary part of $I^{(k_1,k_2)}(y_1,z_1)$ can be written as

$$
\begin{aligned}
\Im I^{(k_1,k_2)}(y_1,z_1) = \; & 2\pi \left(\frac{\partial^2 (x_1^{(k_1)} - x_1^{(k_2)})}{\partial {y_1}^2} \right)^{-1} \left(\frac{\partial k_1^2}{\partial x_1} \right)^{-1} \left| \frac{\partial k_2^2}{\partial x_1} \right|^{-1} \\
& \times (\tilde{h}(x_1^{(k_1)},y_1,z_1) + \tilde{h}(x_1^{(k_1)},y_1,z_1)) \frac{(y_1 - y_1^{(k_1,k_2)})}{(y_1 - y_1^{(k_1,k_2)})^2 + i\tilde{\epsilon}} ,
\end{aligned}
\tag{B7}
$$

where $h = (y_1 - y_1^{(k_1,k_2)})\tilde{h}$. Integrating $\Im I^{(k_1,k_2)}$ with respect to y_1 and letting $\tilde{\epsilon} \to 0$ gives

$$
\int_0^1 dy_1 \Im I^{(k_1,k_2)}(y_1,z_1) = \wp \int_0^1 dy_1 \Im I^{(k_1,k_2)}(y_1,z_1) ,
\tag{B8}
$$

i.e., only the principle-value part of the integration survives. The principle-value integral in Eq. (B8) can be treated analogous to the principle-value integrals in x_1 (cf. Eq. (B3)).

Proceeding along the steps outlined in this appendix, i.e. carefully separating the singular contributions, exploiting delta functions, rewriting principal-value integrals as ordinary integrals plus analytically solvable principle-value integrals, it is finally possible to do all the

numerical integrations by means of fixed-point Gaussian quadrature. For our purposes an x-y-z grid of $20 \times 20 \times 24$ turned out to be sufficient. Taking instead a $32 \times 32 \times 48$ grid changes the results by less than 0.2%. The numerical calculations were performed on a DEC7000-610 APLPHA workstation. For the larger grid size the calculation of $d\sigma/dt(\gamma \mathrm{p} \rightarrow \mathrm{K}^{+}\Lambda)$ took about 1 second per energy point and angle.

REFERENCES

* E-mail: kroll@wpts0.physik.uni-wuppertal.de

** Present address: Deutsche Bank, Frankfurt

+ E-mail: passek@thphys.irb.hr

++ E-mail: schweigerw@edvz.kfunigraz.ac.at

[1] C. Bennhold, Phys. Rev. C **39**, 1944 (1989).

[2] R. A. Adelseck and B. Saghai, Phys. Rev. C **42**, 108 (1990); **45**, 2030 (1992).

[3] R. A. Williams, C. R. Ji, and S. R. Cotanch, Phys. Rev. C **46**, 1617 (1992).

[4] T. Mart, C. Bennhold, and C. E. Hyde-Wright, Phys. Rev. C **51**, R1074 (1995).

[5] R. A. Schumacher, Nucl. Phys. **A585**, 63c (1995).

[6] E. Paul *et al.*, Prog. Part. Nucl. Phys. **34**, 201 (1995).

[7] Z. Li, Phys. Rev. C **52**, 1648 (1995).

[8] A. Donnachie, in *High Energy Physics* V, edited by E. H. S. Burhop (Acadenic Press, New York - London, 1972).

[9] J. F. Gunion, S. J. Brodsky, and R. Blankenbecler, Phys. Rev. D **8**, 287 (1973).

[10] For a review of hard exclusive processes and further references see, e.g., S. J. Brodsky and G. P. Lepage, in *Perturbative Quantum Chromodynamics*, edited by A. H. Mueller (World Scientific, Singapore, 1989).

[11] V. L. Chernyak and A. R. Zhitnitsky, Phys. Rep. **112**, 173 (1984).

[12] G. R. Farrar, H. Zhang, A. A. Ogloblin, and I. R. Zhitnitsky, Nucl. Phys. **B311**, 585 (1988).

[13] V. L. Chernyak, A. A. Ogloblin, and I. R. Zhitnitsky, Z. Phys. C **42**, 569 (1989).

[14] N. G. Stefanis, Acta Phys. Pol. B **25**, 1777 (1994).

[15] R. Jakob, P. Kroll, and M. Raulfs, J. Phys. G **22**, 45 (1996).

[16] J. Bolz and P. Kroll, preprint **WU B 95-35**, Wuppertal (1996).

[17] V. Braun and I. Halperin, Phys. Lett. **B328**, 457 (1994).

[18] A. Radyushkin, Nucl. Phys. B**325** (1991) 141c.

[19] G. R. Farrar, K. Huleihel, and H. Zhang, Nucl. Phys. **B349**, 655 (1991).

[20] R. Jakob, P. Kroll, M. Schürmann, and W. Schweiger, Z. Phys. **A347**, 109 (1993).

[21] P. Kroll, Th. Pilsner, M. Schürmann, and W. Schweiger, Phys. Lett. **B316**, 546 (1993).

[22] P. Kroll, M. Schürmann, and P. A. M. Guichon, Wuppertal preprint WU B 95-09 (1995), to be published in Nucl. Phys. A.

[23] R. Jakob, Phys. Rev. D **50**, 5647 (1994).

[24] M. Anselmino, P. Kroll, and B. Pire, Z. Phys. **C36**, 89 (1987); P. Kroll, in *Proceedings of the Adriatico Research Conference on Spin and Polarization Dynamics in Nuclear and Particle Physics*, Trieste, Italy, 1988.

[25] E. V. Shuryak, Phys. Rep. **115**, 151 (1984).

[26] M. Virchaux and A. Milsztajn, Phys. Lett. **B274**, 221 (1992).

[27] M. Szczekowski, in *Proceedings of the Intern. Workshop on Quark Cluster Dynamics, Bad Honnef (1992)*, Lecture Notes in Physics **417**, edited by K. Goeke, P. Kroll, and H. Petry (Springer, Berlin-Heidelberg, 1993).

[28] N. G. Stefanis, Phys. Rev. D **40**, 2305 (1989).

[29] M. Benayoun and V. L. Chernyak, Nucl. Phys. **B329**, 285 (1990).

[30] B. Chibisov and A. R. Zhitnitsky, Phys. Rev. D **52**, 5273 (1995).

[31] T. Huang, Nucl. Phys. [Proc. Suppl.] **B7**, 320 (1989).

[32] J. D. Bjorken and S. D. Drell, *Relativistic Quantum Fields* (McGraw-Hill, New York, 1965).

[33] I. S. Barker, A. Donnachie, and J. K. Storrow, Nucl. Phys. **B95**, 347 (1975).

[34] F. Tabakin, Nucl. Phys. **A570**, 311c (1994).

[35] J. Küblbeck, M. Böhm, and A. Denner, Comp. Phys. Commun. **60**, 165 (1990).

[36] R. Mertig, M. Böhm, and A. Denner, Comp. Phys. Commun. **64**, 345 (1991).

[37] R. Kleiss and W. J. Stirling, Nucl. Phys. **B262**, 235 (1985).

[38] M. Schürmann, Thesis WUB-DIS 92-4 (1992).

[39] J. A. M. Vermaseren, *Symbolic Manipulation in FORM* (Computer Algebra Nederland, Amsterdam, 1991).

[40] R. L. Anderson *et al.*, Phys. Rev. D **14**, 679 (1976).

[41] S. Ong, Phys. Rev. D **52**, 3111 (1995).

[42] A. S. Kronfeld and B. Nižič, Phys. Rev. D **44**, 3445 (1991).

[43] G. R. Farrar, G. Sterman, and H. Zhang, Phys. Rev. Lett. **62**, 2229 (1989).

[44] G. Vogel *et al.*, Phys. Lett. **B40**, 513 (1972).

[45] W. A. Crabb *et al.*, Phys. Rev. Lett. **65**, 3241 (1990).

[46] G. Bunce *et al.*, Phys. Rev. Lett. **36**, 1113 (1976).

[47] J. Arvieux and B. Pire, Prog. Part. Nucl. Phys., **35**, 299 (1995).

FIGURES

FIG. 1. Constituent kinematics for $\gamma p \longrightarrow K^{(*)+}\Lambda$.

FIG. 2. A few representative examples of Feynman diagrams contributing to the elementary process $\gamma u S_{[u,d]} \longrightarrow u\bar{s}s S_{[u,d]}$.

FIG. 3. Differential cross section for $\gamma p \longrightarrow K^+\Lambda$ scaled by s^7 vs. $\cos(\theta_{cm})$. Solid (dash-double-dotted) line: diquark-model result at $p^{\gamma}_{lab} = 6\,\mathrm{GeV}$ ($4\,\mathrm{GeV}$), proton and Lambda DAs chosen according to Eq. (2.12), Kaon DA according to Eq. (2.8) (asymptotic DA); short-dashed line: diquark-model result at $p^{\gamma}_{lab} = 6\,\mathrm{GeV}$, proton and Lambda DAs chosen according to Eq. (2.12), Kaon DA according to Eq. (2.9) (Chernyak-Zhitnitsky DA [11]); long-dashed line: quark-model result [19] for the asymmetric proton and Lambda DAs of Ref. [12] and the Kaon DA Eq. (2.9). Experimental data are taken from Ref. [40].

FIG. 4. Diquark model predictions for the non-vanishing $\gamma p \longrightarrow K^+\Lambda$ polarization observables. Full (short-dashed) line: same as in Fig. 3.

FIG. 5. Differential cross section for $\gamma p \longrightarrow K^+\Lambda$ scaled by s^7 vs. $\cos(\theta_{cm})$ at $p^{\gamma}_{lab} = 6\,\mathrm{GeV}$ – contributions of the helicity amplitudes S_1 and S_2, respectively. Solid (long-dashed) line: contribution of S_1 (S_2) for proton and Lambda DAs chosen according to Eq. (2.12), Kaon DA according to Eq. (2.8); short-dashed (dash-dotted) line: contribution of S_1 (S_2) for proton and Lambda DAs chosen according to Eq. (2.12), Kaon DA according to Eq. (2.9).

FIG. 6. Phases of the helicity amplitudes S_1 and S_2, respectively. Lines as in Fig. 5.

FIG. 7. Differential cross section for $\gamma p \longrightarrow K^{*+}\Lambda$ scaled by s^7 vs. $\cos(\theta_{\rm cm})$ at $p^{\gamma}_{\rm lab} = 6\,{\rm GeV}$. Solid line: diquark-model prediction, proton and Lambda DAs chosen according to Eq. (2.12), K^* DA according to Eq. (2.8) (asymptotic DA); short-dashed line: diquark-model prediction, proton and Lambda DAs chosen according to Eq. (2.12), K^* DA according to Eqs. (2.10) and (2.11) (taken from Ref. [29]).

TABLES

TABLE I. Propagator-pole positions, x_1-derivatives, and principal value integrals for the singular propagators occurring in Eq. (3.9).

k^2	$x_1^{(k)}$	$\frac{\partial k^2}{\partial x_1}$	$\wp\int_0^1 \frac{dx_1}{k^2}$
g_1^2	$\dfrac{z_1\hat{t}}{\hat{t}+z_2\hat{u}}$	$-(\hat{t}+z_2\hat{u})$	$\dfrac{-1}{\hat{t}+z_2\hat{u}}\ln\left(\dfrac{-z_2\hat{s}}{z_1\hat{t}}\right)$
g_2^2	$\dfrac{-y_1\hat{s}}{y_1\hat{t}+\hat{u}}$	$(y_1\hat{t}+\hat{u})$	$\dfrac{-1}{y_1\hat{t}+\hat{u}}\ln\left(\dfrac{-y_1\hat{s}}{y_2\hat{u}}\right)$
q_2^2	$\dfrac{y_2z_1\hat{t}+y_1z_2\hat{u}}{y_2\hat{t}+z_2\hat{u}}$	$-(y_2\hat{t}+z_2\hat{u})$	$\dfrac{-1}{y_2\hat{t}+z_2\hat{u}}\ln\left(\dfrac{-y_2z_2\hat{s}}{y_2z_1\hat{t}+y_1z_2\hat{u}}\right)$
q_3^2	$\dfrac{y_2z_2\hat{t}+y_1z_1\hat{u}}{y_2\hat{t}+z_1\hat{u}}$	$-(y_2\hat{t}+z_1\hat{u})$	$\dfrac{-1}{y_2\hat{t}+z_1\hat{u}}\ln\left(\dfrac{-y_2z_1\hat{s}}{y_2z_2\hat{t}+y_1z_1\hat{u}}\right)$
q_4^2	$\dfrac{-y_1z_2\hat{s}}{y_1\hat{t}+z_2\hat{u}}$	$(y_1\hat{t}+z_2\hat{u})$	$\dfrac{-1}{y_1\hat{t}+z_2\hat{u}}\ln\left(\dfrac{-y_1z_2\hat{s}}{y_1z_1\hat{t}+y_2z_2\hat{u}}\right)$
q_5^2	$\dfrac{-y_1z_1\hat{s}}{y_1\hat{t}+z_1\hat{u}}$	$(y_1\hat{t}+z_1\hat{u})$	$\dfrac{-1}{y_1\hat{t}+z_1\hat{u}}\ln\left(\dfrac{-y_1z_1\hat{s}}{y_1z_2\hat{t}+y_2z_1\hat{u}}\right)$
D_1^2	$\dfrac{y_1z_1\hat{t}+y_2z_2\hat{u}}{y_1\hat{t}+z_2\hat{u}}$	$-(y_1\hat{t}+z_2\hat{u})$	$\dfrac{-1}{y_1\hat{t}+z_2\hat{u}}\ln\left(\dfrac{-y_1z_2\hat{s}}{y_1z_1\hat{t}+y_2z_2\hat{u}}\right)$
D_2^2	$\dfrac{-y_2z_1\hat{s}}{y_2\hat{t}+z_1\hat{u}}$	$(y_2\hat{t}+z_1\hat{u})$	$\dfrac{-1}{y_2\hat{t}+z_1\hat{u}}\ln\left(\dfrac{-y_2z_1\hat{s}}{y_2z_2\hat{t}+y_1z_1\hat{u}}\right)$

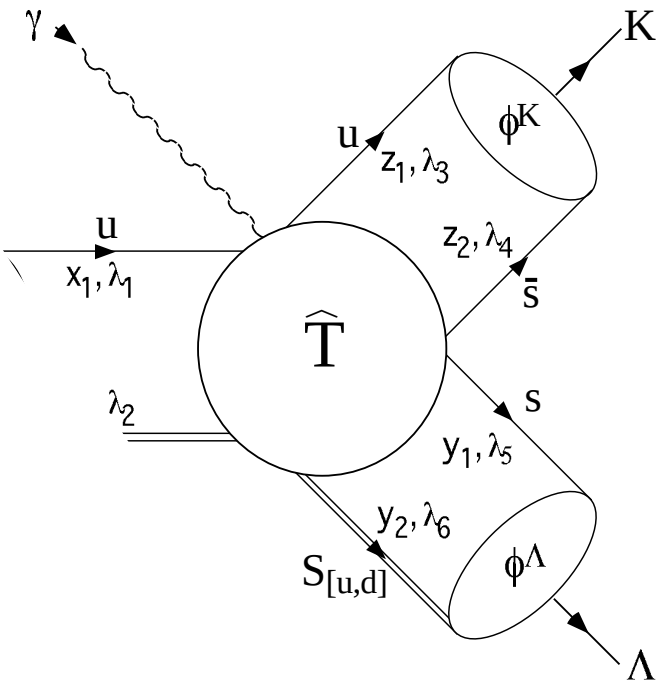

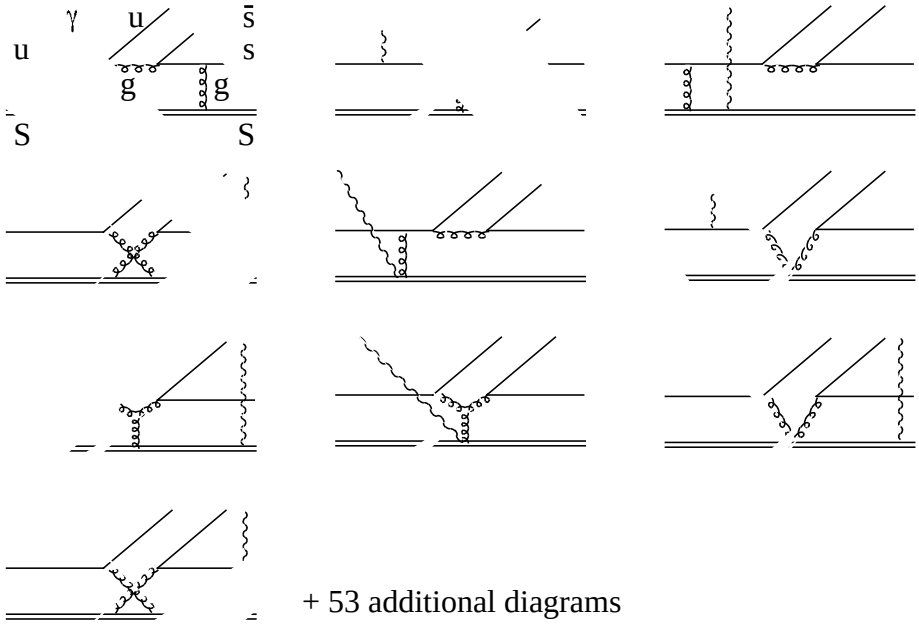

+ 53 additional diagrams

Figure 2

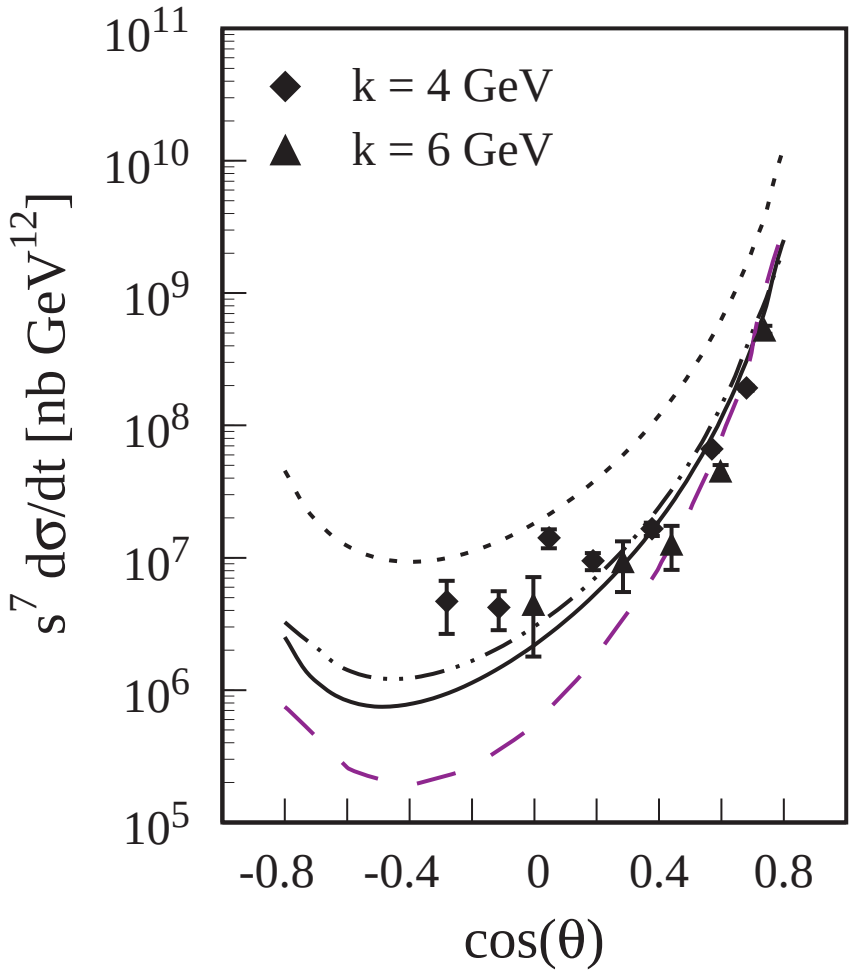
k = 4 GeV
k = 6 GeV
10^{11}
10^{10}
10^{9}
10^{8}
10^{7}
10^{6}
10^{5}
$s^7\ d\sigma/dt\ [nb\ GeV^{12}]$
-0.8
-0.4
0
0.4
0.8
cos(θ)

Figure 3

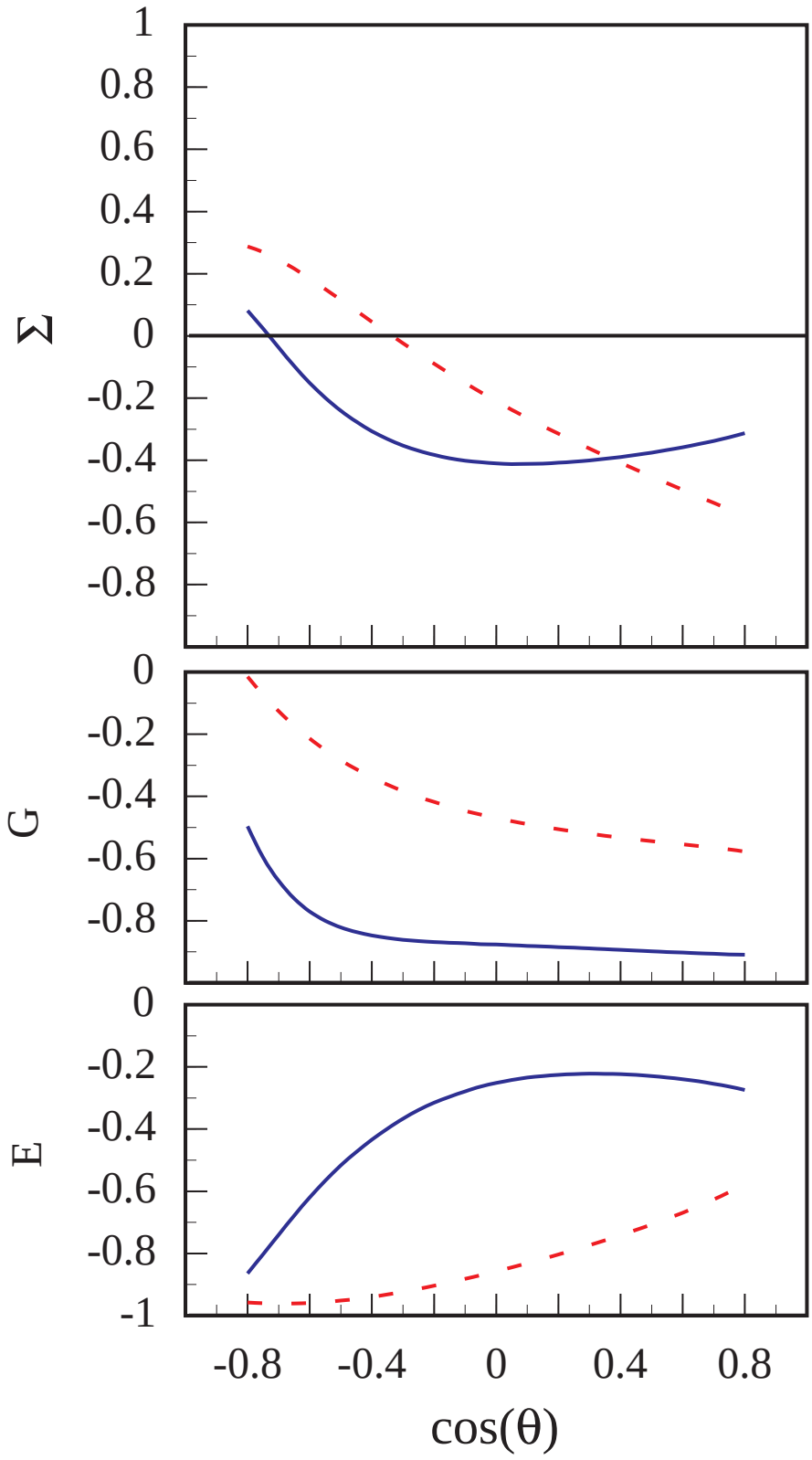
1
0.8
0.6
0.4
0.2
0
-0.2
-0.4
-0.6
-0.8
Σ
0
-0.2
-0.4
-0.6
-0.8
G
0
-0.2
-0.4
-0.6
-0.8
-1
E
-0.8
-0.4
0
0.4
0.8
cos(θ)

Figure 4

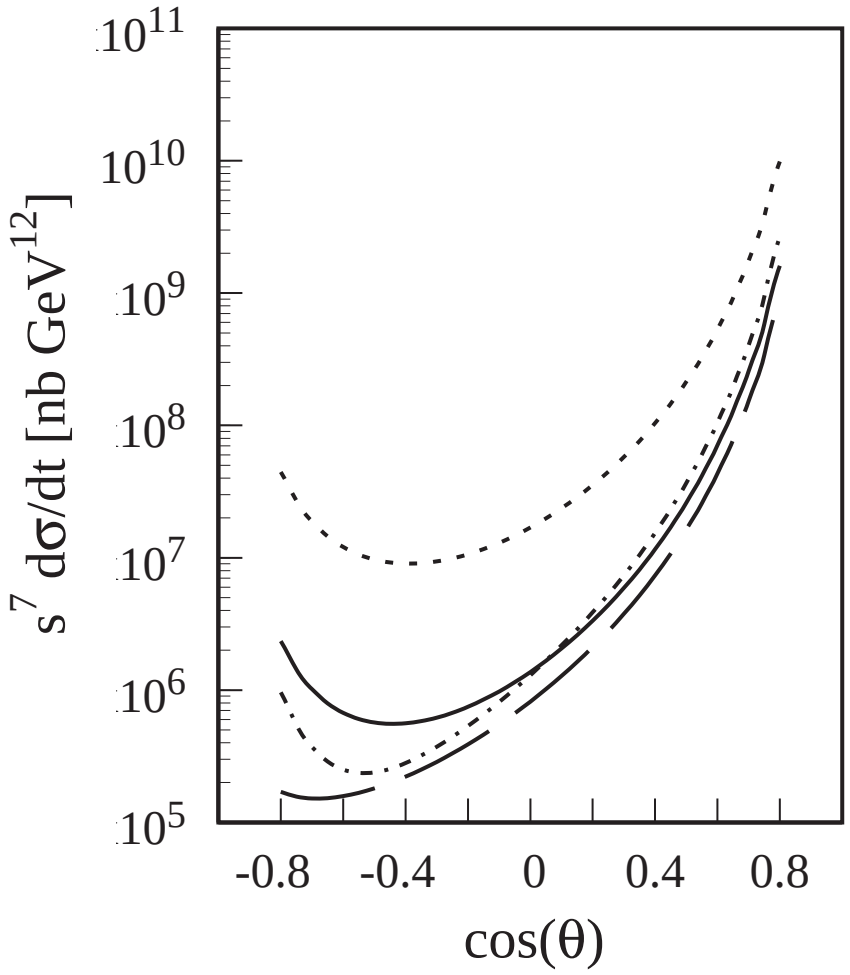
10^{11}
10^{10}
10^{9}
10^{8}
10^{7}
10^{6}
10^{5}
$s^7\ d\sigma/dt\ [nb\ GeV^{12}]$
-0.8
-0.4
0
0.4
0.8
cos(θ)

Figure 5

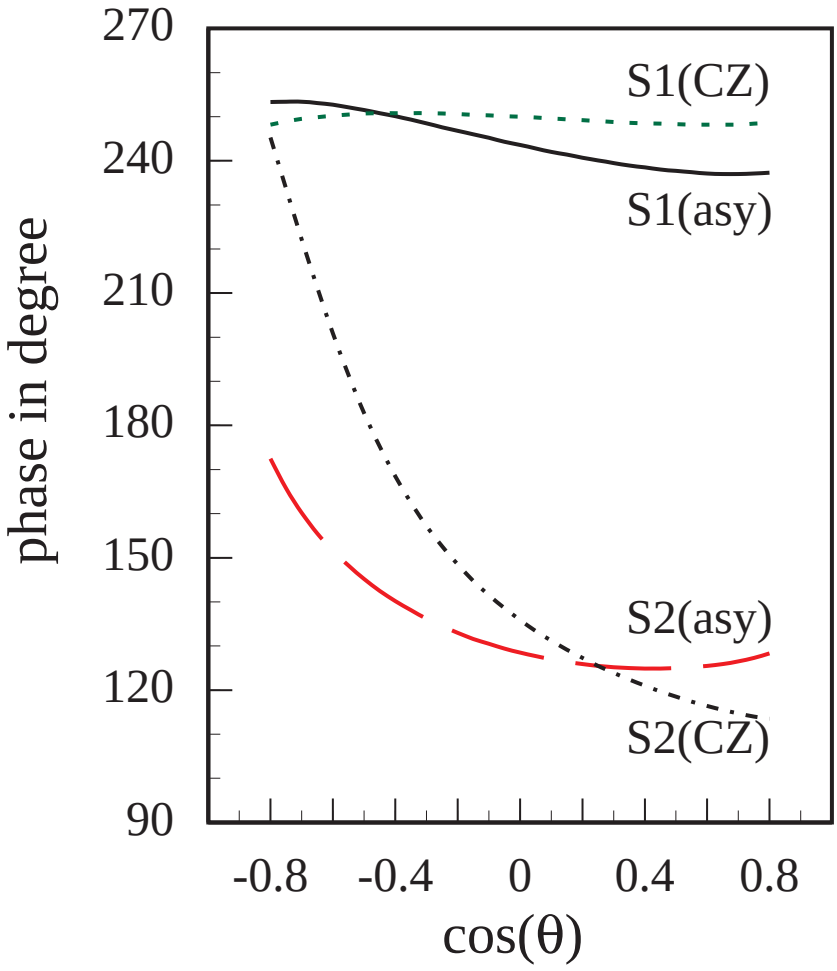
270
240
210
180
150
120
90
phase in degree
S1(CZ)
S1(asy)
S2(asy)
S2(CZ)
-0.8
-0.4
0
0.4
0.8
cos(θ)

Figure 6

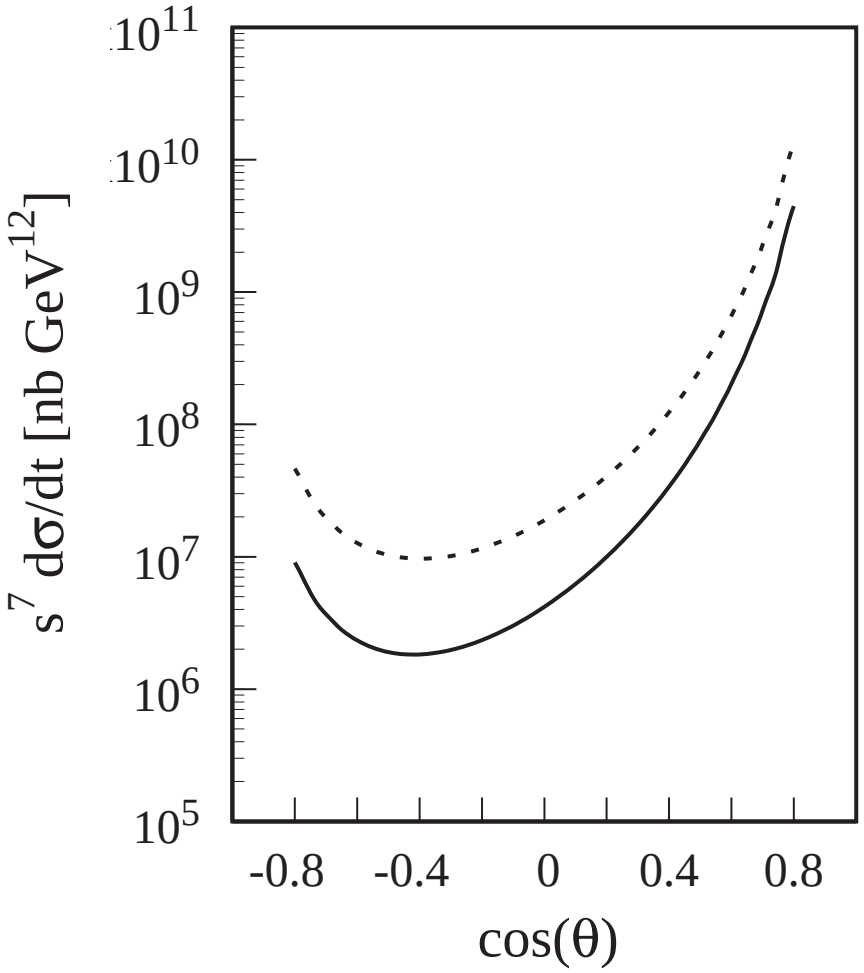

Figure 7